Check for updates

ADVANCED OPTICAL MATERIALS
www.advopticalmat.de

Ribbontail Stingray Skin Employs a Core–Shell Photonic Glass Ultrastructure to Make Blue Structural Color

Venkata A. Surapaneni, Michael J. Blumer, Kian Tadayon, Ashlie J. McIvor, Stefan Redl, Hanne-Rose Honis, Frederik H. Mollen, Shahrouz Amini, and Mason N. Dean**

Structural blue colors are common in animals, with the tissue nanostructures and material systems that produce them—especially bright blues—typically based on highly ordered nano-architectures. In this study, we describe an unusually bright and angle-independent structural blue from the skin of ribbontail stingray, arising from a more disordered array of scattering elements with a previously undescribed core–shell ultrastructure, involving nano-vesicles enclosing guanine nano-platelets. We show that this skin architecture functions as an intracellular photonic glass, coherently scattering blue, while broadband absorption from closely associated melanophores obviates the low color saturation typical for photonic glasses. Our characterization of skin ultrastructure and color in a stingray demonstrates how disordered systems can be harnessed to produce brilliant hues while illustrating that the capacity for guanine-based colors likely arose extremely early in vertebrate evolution. Moreover, the material-structure-function associations underlying ribbontail stingray coloration, employing two distinct photonic phenomena, illustrate how the evolution of nanoscale architectures can have profound effects at much larger size scales (e.g., in visual ecology and communication), and provide fundamental guidelines for color-saturated manmade photonic glasses.

1. Introduction

The colors of living organisms are diverse and can play crucial roles in communication, predator evasion, and thermoregulation.[1] The various mechanisms nature uses to produce color, therefore, can offer fundamental insights into the biological tools that shape diverse ecological interactions, as well as the physical and phylogenetic relationships that govern them. Color in nature can be either due to selective "absorption" of light by pigments (pigmentary color), selective "scattering" of light from nanoscale structures (structural color), or a combination of these mechanisms. In particular, blue colors are of special interest, being widespread, visually perceived by many taxa, and involved in a variety of functions. Pigmentary blues are however extremely uncommon, meaning most natural blues have a structural origin.[2,3] Yet, the exact nanostructural features and materials responsible for producing natural blues vary considerably across taxa, indicating that nature has arrived at multiple solutions for creating similar striking colorations. Many bony fishes, for example, especially shallow water and reef-associated species, have diverse blue color patterns,[4-6] derived from pigmentary and purine-containing cells.[7-10] In contrast, the blue skin colorations that have been anecdotally described in multiple disparate species of sharks and rays (elasmobranch fishes [11,12]) have yet to

V. A. Surapaneni, M. N. Dean
Department of Infectious Diseases and Public Health
City University of Hong Kong
Kowloon HKG, Hong Kong
E-mail: amar.sv@cityu.edu.hk; mndean@cityu.edu.hk
V. A. Surapaneni, S. Amini, M. N. Dean
Department of Biomaterials
Max Planck Institute of Colloids and Interfaces
14476 Potsdam, Germany

The ORCID identification number(s) for the author(s) of this article can be found under https://doi.org/10.1002/adom.202301909

© 2024 The Authors. Advanced Optical Materials published by Wiley-VCH GmbH. This is an open access article under the terms of the Creative Commons Attribution License, which permits use, distribution and reproduction in any medium, provided the original work is properly cited.

DOI: 10.1002/adom.202301909

M. J. Blumer, H.-R. Honis
Institute of Clinical and Functional Anatomy
Medical University Innsbruck
Innsbruck 6020, Austria
K. Tadayon
B CUBE – Center for Molecular Bioengineering
Technische Universität
01307 Dresden, Germany
A. J. McIvor
MARE – Marine and Environmental Sciences Centre
Regional Agency for the Development of Research, Technology and Innovation (ARDITI)
Funchal 9020-105, Portugal
S. Redl
Institute of Neuroanatomy
Medical University Innsbruck
Innsbruck 6020, Austria
F. H. Mollen
Elasmobranch Research
Bonheiden 2820, Belgium

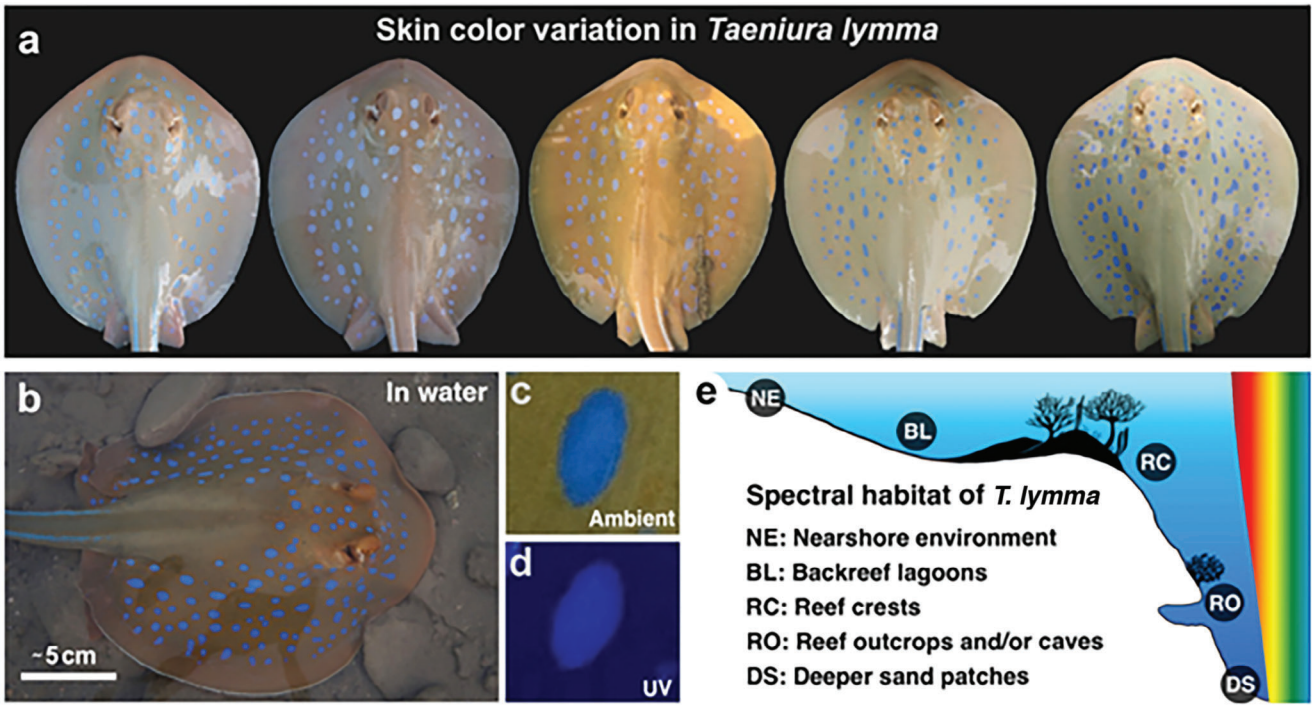

Figure 1. Skin color and habitat of ribbontail stingray *Taeniura lymma*: a) The natural variation we have observed in the skin color of ribbontail stingrays, in the blue spots as well as in non-blue regions, suggests variability in the color-producing tissue, whether structural or pigmentary or both. b–c) In a typical color variant in ambient light, the spots and non-blue skin regions appear bright electric blue and green–brown respectively. d) Under a UV light source, the spots are saturated with a strong electric blue hue and other skin regions appear dark blue. e) Ribbontail stingrays occupy a variety of spectral habitats, with changing availability of visible spectrum wavelengths as a function of depth, shown on the right of the image—the blue wavelengths available in all of these regions suggest that the blue spots on the skin of this stingray are ecologically relevant.

be examined. Given that modern elasmobranch fishes and bony fishes diverged from a common ancestor hundreds of millions of years ago, and given the major intrinsic differences in elasmobranch skin, scale, and skeletal structure relative to those of bony fishes, we hypothesized that the blues of sharks and rays very likely represent novel structural color mechanisms for fishes (although, alternatively, a mechanistic convergence with bony fish colorations would be equally exciting).

In this study, we explored the ultrastructure and basis of color production of the skin of the blue-spotted ribbontail stingray, *Taeniura lymma* (Fabricius, ex Forsskål [13]) (**Figure** 1a–d), a small benthic ray common to coral reef habitats across the Indo-West Pacific from South Africa to Papua New Guinea.[12,14] Juvenile rays typically occupy shallow reef-adjacent and intertidal habitats (i.e., mangrove, seagrass, and rocky shorelines,[15-17] Figure 1e: NE, BL and RC; down to 5 m depth), whereas adults are often found in deeper reef environments (Figure 1e: RO and DS; down to 50m depth), but also utilize shallow sandflats for foraging, mating, and pupping.[14-18] Daily activity patterns for *T. lymma* are largely unknown but are likely influenced by environmental cues such as photoperiod, temperature, and tide, with an increased activity level around dusk, similar to other batoids.[19-21] As with other batoids, *T. lymma* is also expected to be active throughout the day, meaning that the visual perception of the colors of their skin should vary significantly due to changing light conditions. Unlike the relatively uniform and muted body colors of many oceanic stingrays, the ribbontail stingray has a conspicuous color pattern, with bright electric blue coloration, accenting its dorsal body skin color [12]; our field studies show substantial color variation in both the blue and non-blue regions, with the latter ranging from greenish– to yellowish–brown to even orange dorsal body skin (Figure 1a–d). In providing a mechanistic description of color in an elasmobranch fish, we also demonstrate structural color for the first time in this group and characterize what we believe to be a novel cell type responsible for color production.

2. Results and Discussion

2.1. Visual and Optical Properties of the Blue Spots

Natural color is a product of context: of incident light wavelengths, the properties of the color-producing tissue (which dictate the range of wavelengths reflected), and the position and sensory capabilities of the observer, whether predator, prey, or potential mate. Given the use of multiple reef microhabitats by the ribbontail stingray, one can assume variations in the spectral habitat that the species may occupy [22] (Figure 1e). For instance, in-water light transmission and attenuation typically increase from backreef to forereef waters, with blue and green wavelengths dominating in eutrophic coastal waters and lagoons, and greater availability of blue wavelengths when moving to the forereef and offshore waters [22,23] (Figure 1e, spectra). These differences in light availability can also be affected by natural variations in suspended particulates and dissolved organic matter and may lead to

© 2024 The Authors. Advanced Optical Materials published by Wiley-VCH GmbH

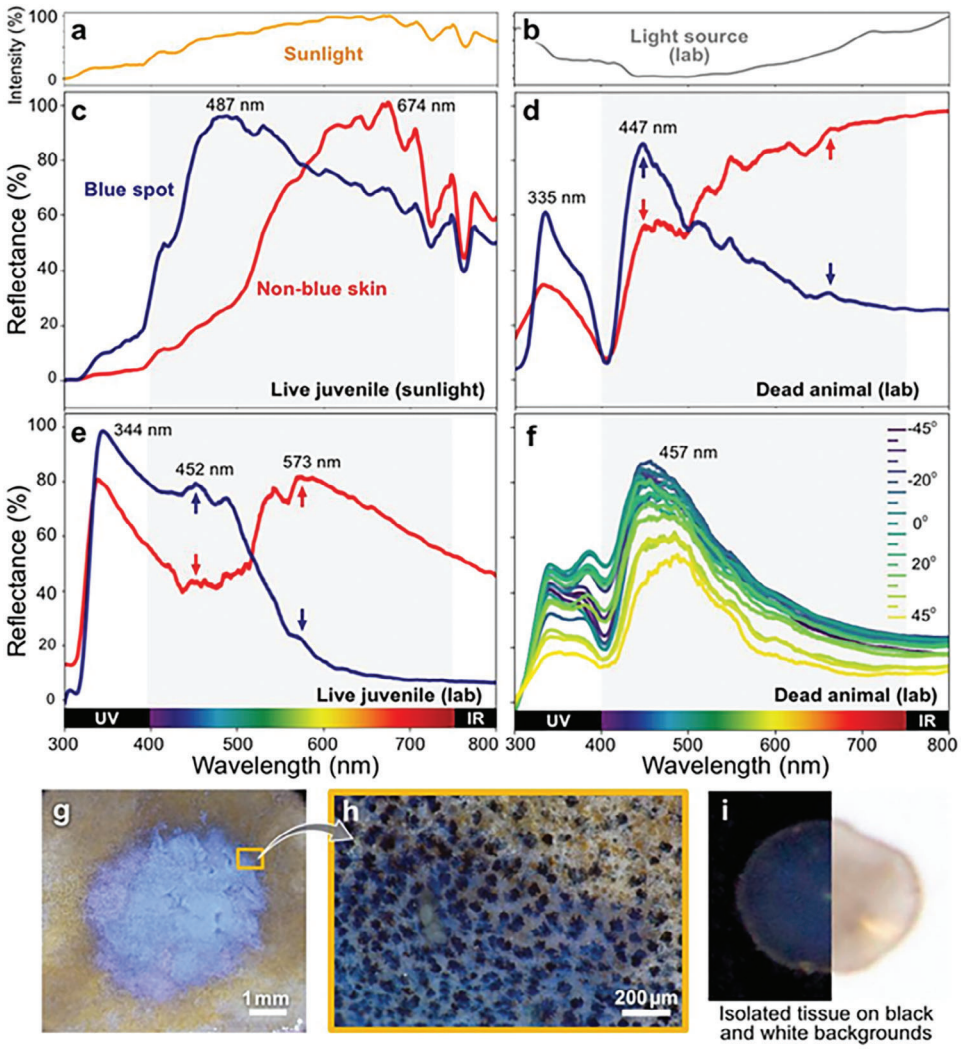

Figure 2. Color properties of ribbontail stingray skin in water: The blue and non-blue regions of ribbontail stingray skin showed strong variation in the wavelengths reflected, whether in a) sunlight or b) lab conditions. The normalized reflectance plots showed that c) in sunlight, the spots on the skin of a live juvenile reflect strongly in the blue–cyan region, while the non-blue regions reflect yellow–red wavelengths of the visible spectrum. d–e) Lab measurements showed a strong reflection of short wavelengths (blue) and strong absorption of long wavelengths from the spots (blue arrows), but vice versa from the non-blue skin regions (red arrows). All skin regions, however, strongly reflected UV wavelengths. f) Reflectance measurements at various angles of incidence on the skin of the adult specimen demonstrated the non-iridescent color of spots. g) The blue spot color had a milky paste-like quality upon closer inspection, and h) at higher magnifications, could be seen to involve a superficial blue layer underlain by numerous black splotches that extended only sparsely into the non-blue region (upper right corner of h). i) Excised superficial skin tissue placed on black carbon tape (left) versus a white background (right) showed that a black background is necessary for the blue color of the skin.

variations in the color perception of the ribbontail stingray across local and regional scales.[23,24] Understanding how natural color varies with context can therefore provide critical baseline information, not only on the properties and basis of color production but also on the role that skin color plays in an animal's ecology and its structural and/or compositional stability.

In this study, all sampled specimens, including both juvenile and adult stingrays, exhibited the bright electric blue coloration distinctive for this species, displaying spots on their dorsal body, lateral stripes on their tails, and an ovular swath of color surrounding the lower caudal fin fold to the tip of the tail and the stinging spine (Figure 1b). Color profile measurements on ribbontail stingray skin in water showed that, in sunlight (**Figure** 2a; Figure S1a, Supporting Information), the juvenile animal's blue spots exhibited peaks in the blue region (≈487 nm), while the non-blue portions of skin reflected most strongly in the yellow-red region (≈674 nm) (Figure 2c). In lab conditions (i.e., under a controlled range of incident wavelengths, Figure 2b; Figure S1a, Supporting Information), the trend was similar, where the blue spots predominantly reflected short wavelengths in the blue–cyan region of the visible spectrum (juvenile: ≈452 nm; adult: 447 nm), whereas the non-blue regions reflected longer wavelengths. Surprisingly, a strong UV peak (juvenile: ≈344 nm and adult: ≈335 nm) was common to both blue and non-blue regions of the skin (Figure 2d,e). This variation between sunlight and lab measurements is likely due to the nature of the incident light in

© 2024 The Authors. Advanced Optical Materials published by Wiley-VCH GmbH

the two conditions, being directional and broad-spectrum in the lab, but diffuse with more variable wavelengths in ambient conditions (Figure 2a–e; Figure S1b, Supporting Information). Measurements at various angles of light incidence indicated that the blue spots are non-iridescent, confirming our visual observations from intact specimens that the color is unchanging with viewing angle (Figure 2f; Figure S1c,d, Supporting Information). Although non-iridescence is often taken to indicate a lack of structural color, it can also be due to an irregularity of the structure [25] that results in scattering of light, regardless of the angle of incidence (see section 2.3); we explore these options at a tissue level below.

The ecology and visual capabilities of this species provide some suggestions as to the roles its electric blue coloration may play for this species. Ribbontail stingrays can perceive blue wavelengths with absorbance maxima at wavelengths ≈479 nm (S-cone photoreceptor cells), 500 nm (rod cells), and 557 nm (L-cone cells).[26] Moreover, the ribbontail stingray has a specialized visual apparatus for low-light scotopic vision and a greater spatial resolving power compared to other benthic batoids,[26,27] which may facilitate improved transmission of visual cues between conspecifics, especially during crepuscular periods where rays are often seen gathered in shallow waters.[17] In these regions, short-wavelength photons dominate the underwater spectrum,[28] where the ambient blue illumination may emphasize and further saturate the blue spot pattern. The mixture of yellow/green and blue coloration in the ribbontail stingray is also an effective color combination that transmits well in reef waters, providing the most chromatic contrast for a range of animal visual systems [29] and possibly serving as an aposematic warning system to nearby predators (supported by the color swath associated with this species' stinging spine). However, given the reduced color-vision range of other reef fish, the conspicuous yellow/green and blue colors of the ribbontail stingray would quickly merge and fade into the background over the span of a few meters towards the achromatic point,[30] suggesting that the blue spot coloration of the ribbontail stingray acts primarily as a near-field signal for inter- or intraspecific communication.

Our observations also demonstrate a uniform reflectance of soft UV (UV-A), suggesting that the components responsible for UV reflection should be identical in both blue and non-blue regions of the skin. This was unexpected and argues the two dominant reflectance peaks (blue and UV) serve different functions. Ribbontail stingray visual pigments block UV radiation [31] and therefore UV reflections from their skin would not be perceived by conspecifics, or even by potential predators (e.g., sharks), since many of those lack UV perception.[31,32] Instead, since behavioral observations show that the ribbontail stingray rarely covers itself in the sand like other stingray species,[14] and since UV-A is not especially damaging to skin and coastal sand is known to reflect UV light (Baltic seaside at Juodkrantė [33]), we hypothesize that the UV-reflectivity of ribbontail stingray skin provides camouflage in sandy, intertidal habitats, perhaps a useful deterrent against predation by birds (which can perceive UV [34]).

On close examination of skin regions with a stereomicroscope, the blue color, especially in the larger body spots, had the quality of a milky paste, dabbed onto the skin surface, with black dendritic splotches coalescing in a dense layer beneath it; this suggested that the regions responsible for the blue color may be quite superficial (Figure 2g,h). The microscale splotches also extended into non-blue regions, albeit only sparsely (Figure 2h). As our specimen lacked skin denticles, the soft nature of its skin allowed us to gently peel away the outer skin layers (≈0.4 mm, with a black spot left behind on the specimen after peeling) and transfer them onto synthetic substrates to explore the effect of the black dendritic layer on the overall color appearance. The isolated tissue, when affixed on a white substrate, was much paler and the tissue was almost transparent, whereas, on black carbon tape, it exhibited a similar blue to that of the intact animal (Figure 2i). Previous studies on biological and artificial optical materials have shown that black backgrounds can serve to absorb longer and incoherently scattered wavelengths and help in the saturation of blue color.[35,36] Similarly in our study, whereas the paler color of ribbontail stingray tissue on white backgrounds suggested a superimposition of all colors in the spectrum, the return of the brighter blue color on black carbon tape indicated that the tissue's natural black backing acts as a broadband absorber of longer wavelengths and is therefore an important component of the blue coloration.

In contrast to our fresh specimens, in one specimen that was frozen immediately after death for ≈4 years, all characteristic blue regions were dark blue or nearly black in color. Strikingly, however, spots cut from this hugely shriveled specimen returned to their natural electric blue immediately when placed in water; moreover, this color switching was reversible, with the blue being recoverable even after multiple freeze-thaw cycles (Figure S2a–c, Supporting Information). Likewise, in the tissue affixed to black carbon tape, the color reversal process was repeatedly achieved following de-/rehydration cycles, with the drying of the tissue producing black and re-wetting recovering blue hues, respectively. In fact, even after being left dry at room temperature for six months, the color of the excised tissue returned to blue soon after rehydration (Figure S2d, Supporting Information). Tissue colors that vary with hydration can be the result of changes in structure and/or refractive index when water leaves the tissue,[37,38] or changes in pigmentary chemistry arising from pH differences.[39] Our observations that the blue skin color of ribbontail stingray is highly robust and reversible with de- and re-hydration were not enough to prove a structural origin of color—thus, tissue-level characterizations were necessary.

2.2. Unique Ultrastructure of Blue Spots of Ribbontail Stingray Skin

The skin of all vertebrates contains specialized color-producing cells called chromatophores. Chromatophores exist in various forms: light-absorbing pigment-containing melanophores (black or brown pigments); erythrophores (red or yellow pigments); cyanophores (blue pigments); and colorless, reflective, and purine-containing leucophores and iridophores.[7–9] The distribution of these cells in skin layers (epidermis and dermis) and their interactions with other tissue components are responsible for the diverse and colorful patterns of fish skin.[2,40,41]

Despite the deep interest in the denticle morphology and hydrodynamics of shark skin,[42,43] the histology of shark and ray skin is surprisingly poorly described. Our light and transmission electron microscopy investigations (**Figure 3**a–j) showed

© 2024 The Authors. Advanced Optical Materials published by Wiley-VCH GmbH

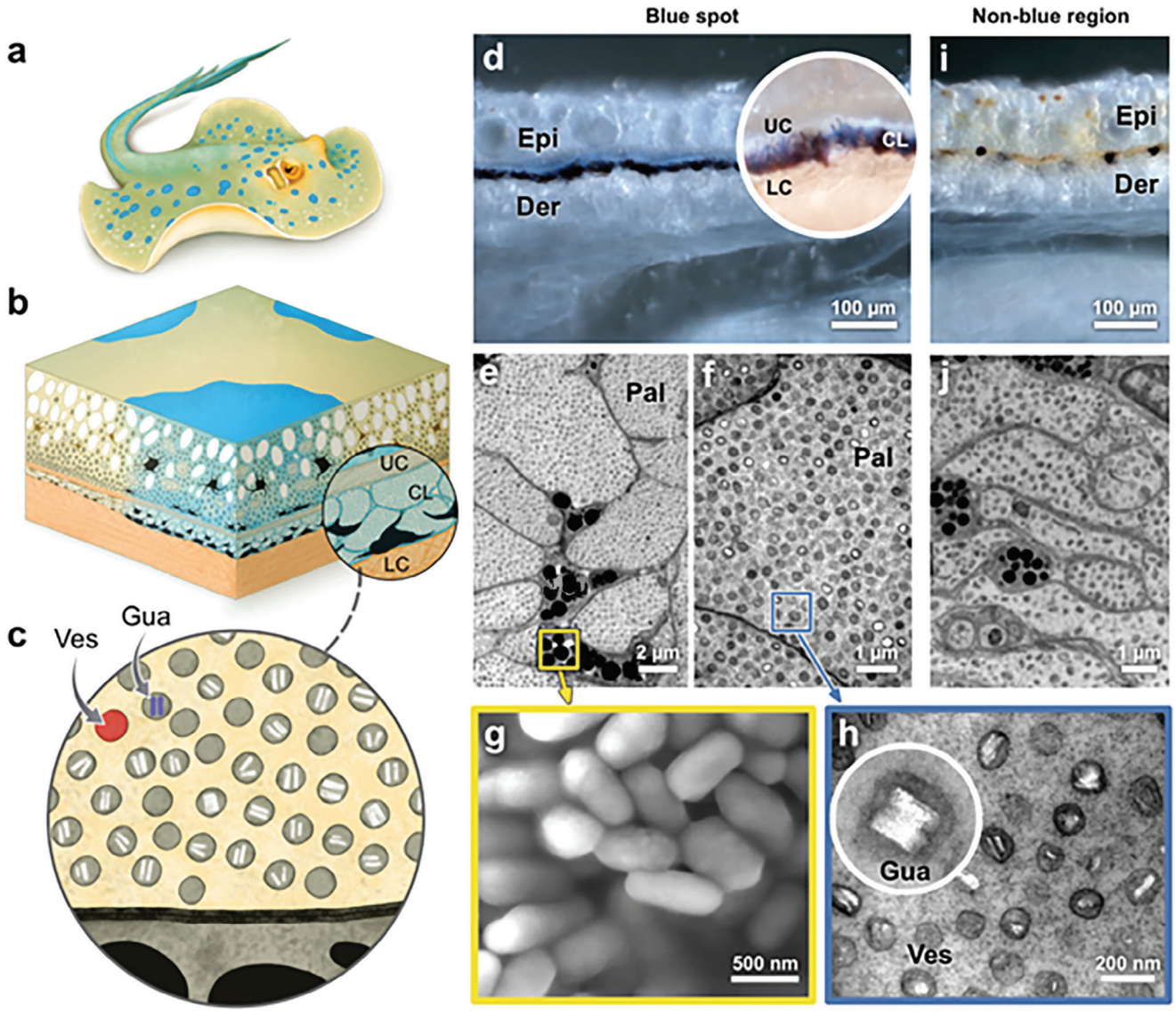

Figure 3. A schematic of a blue spotted ribbontail stingray skin: a–c) shows multiple levels of hierarchical architecture responsible for blue color production. The figure compares the ultrastructure of blue regions (d–h) with non-blue regions (i–j). d) Epi-illuminated blue spots showed a blue hue just above the dark melanin region, sandwiched between the epidermis (Epi) and dermis (Der) suggesting that the source of the blue color is tightly associated with the melanin layer. e,f,h) TEM and g) SEM characterization showed that in the blue spots, in the chromatophore layer (CL) sandwiched between upper (UC) and lower (LC) collagen layers, pale cells (Pal) encase black melanophores (Mel) with g) numerous spherical and ellipsoidal melanosomes. c, e, f, h) The pale cells contain numerous nanovesicles (Ves) surrounded by cytoplasm, the nanovesicles filled with guanine nanoplatelets (Gua), mostly occurring in pairs. The inset in (h) shows a fused pair of platelets in a single vesicle. i, j) Epi-illuminated and TEM images of non-blue skin regions showed fewer and less uniform melanophores in the chromatophore layer (CL) and sparsely distributed vesicles in pale cells.

that, as in other fishes, the skin of ribbontail stingray consists of an epidermis (Epi: 100–250 µm thick), separated from a thicker underlying dermis (Der: 350–500 µm) by a thin basement membrane (B: 0.3 µm). In both blue and non-blue skin regions, the dermis was visibly stratified. A chromatophore layer (CL) with a unique ultrastructure (see below) in the upper dermis was sandwiched between two dense collagenous layers: a thin upper collagen fiber layer (UC, 1–5 µm) below the basement membrane and a thick lower collagen fiber layer (LC, 100–150 µm) of interwoven collagen fiber bundles in the lower dermis (Figure 3a–d,i).

We found three distinct cell types in the skin: mucous cells, melanophores (Mel, with either black or brown pigments, distinct in both histology and TEM), and specialized cells we refer to here as "pale cells" (Pal). These three cell types varied in their arrangement, preponderance, and density in the epidermis and dermis and, more importantly, in ways that distinguished blue from non-blue regions. The epidermis of both blue and non-blue areas were histologically relatively similar, dominated by large mucous cells superficially, but containing a scattered mix of mucous cells, melanophores, and pale cells closer to the basement membrane. We verified that the dark dendritic splotches

© 2024 The Authors. Advanced Optical Materials published by Wiley-VCH GmbH

observed by stereomicroscope (see above) were melanophores, exhibiting stellate morphologies and squeezed between the other cell types (Mel, Figure 3b,d,e). The pale cells were so named because of their nearly featureless appearance in histology/light microscopy , such that they initially looked to be vacuolated (our electron microscopy observations revealed this not to be the case; see below). Although blue and non-blue regions were compositionally similar, the epidermis in the blue regions tended to contain fewer mucus-producing cells in some regions/specimens, more pale cells, and black melanophores [44,45] that were more dendritic and darker (in contrast to the non-blue region, which contained less-electron-dense brown melanophores and more sparsely distributed black melanophores, Figure 3d,i).

Unlike the epidermis, the upper dermis exhibited key ultrastructural differences between blue and non-blue regions of the skin. In blue regions only, the upper dermis (≈35 µm thick) was densely packed with pale cells, amalgamated into large multi-cell complexes which often enclosed branched black melanophores (Figure 3b–e). The tight association of pale cells with melanophores and the extended dendritic processes of the latter resulted in intracellular melanosomes (i.e. within melanophores, Figure 3e,g) being distributed throughout the chromatophore layer, with the local concentration of melanosomes higher deeper in the tissue (corresponding to the "black dendritic backing layer" we observed in the previous section). In contrast, in non-blue regions, the chromatophore layer was only one-third as thick (up to 15 µm wide), contained more sparsely distributed black and brown melanophores, and a continuous layer of pale cells (Figure 3i). The upper and lower collagen layers that surround the chromatophore layer were present in both blue and non-blue regions of the skin with no obvious differences, although the lower collagen layer was slightly thicker in the non-blue region.

Our electron microscopy investigations revealed that pale cells do in fact contain a highly organized internal structure (Figure 3f), which only became visible when samples were carefully and immediately fixed and then contrast-stained. In such samples, the lumen of pale cells was observed to be entirely full of colloid-like nano-vesicles (Ves ≈126.79 ± 13.08 nm in diameter, Figure 3c,e,f,h), the morphology and arrangement of which varied with location in the tissue: whereas pale cells in the non-blue region contained vesicles that were more elongate and random in their arrangement, those in blue skin regions were spherical and mono-disperse with a strikingly uniform arrangement and packing density (≈28 vesicles µm^{-2}, Figure f,j). In the upper dermis of the blue skin regions, intracellular melanosomes were jet black and of variable cross-section, ranging from ellipsoidal to spherical and roughly similar in size (500–600 nm), several times larger than pale cell vesicles (Figure 3e–h). In well-fixed specimens, the extremely tight encasement of pale cells around melanophores was particularly impressive—with the many surrounding pale cells creating a nearly uniform, nano-vesicular corona around each pigment cell. In contrast to the non-blue regions, epi-illuminated light microscopy observations of skin cross-sections showed a conspicuous blue hue in blue spot regions, just above the dense black melanophore layer, suggesting that the blue color originates in the overlying pale cell layer (Figure 3d,i).

TEM observations (supported by SEM imaging) revealed that the spherical nano-vesicles contained crystalline structures (85.01 ± 14.58 nm wide, Figure 3h), often rhomboidal in cross-section. Crystals typically occur in pairs within the matrix of each vesicle, with no defined orientation. EDX and Raman spectroscopic measurements (Figure S3, Supporting Information) confirmed that these nano-crystals were nitrogen-rich and made of anhydrous beta-guanine [46,47] (Gua, Figure 3h). Beta-guanine is a common structural-color-producing purine in bony fishes, typically manifesting as stacks (>10) of long guanine platelets (each tens of µm long and tens of nm thick), inside iridophore cells. During development, the guanine platelets nucleate from an amorphous precursor inside small vesicles in iridophores, grow, and then coalesce to form single crystal platelets. Crystal growth propagates, partitioned by intravesicular bands, resulting in a layered arrangement of long guanine crystals.[48–52] These large crystalline stacks act as multilayer reflectors to produce color and/or a silvery appearance in the skin.[53,54]

Pale cells are clearly a widespread and characteristic cell type in ribbontail stingray skin and, we propose, at least partly responsible for this species' blue coloration. With the exception of black and brown melanophores, we have not observed any pigment cells that might contribute to the blue color in ribbontail stingrays nor found any previous description of pale cells in elasmobranch or bony fishes in the literature; the careful preparations required to visualize pale cell contents, however, could mean these cells are more prevalent than realized, at least in elasmobranchs. Although the distribution and composition of pale cells indicate they are likely involved in a guanine-based blue structural color, the morphology and arrangement of guanine crystals in the cells of ribbontail stingrays are strikingly different from that of bony fishes. To the best of our knowledge, such a uniform and stable colloidal arrangement of guanine nanocrystals embedded in nano-vesicles has never been reported in fishes. Oddly, the most similar example we find in the literature is from an invertebrate, the Spanish shawl nudibranch mollusk (*Flabellina iodinea*), where short stacks of guanine nanocrystals, bound by membranes, form "punctate reflectors." [55] Although these nanoreflectors are also localized in specialized cells near the epithelial basal membrane, as in ribbontail stingray, their vesicles are less organized in their arrangement, instead packed in high densities within their specialized cells, but also scattered and mobile throughout the epithelium. The distinct morphology of ribbontail stingray pale cells argues that their mechanism of guanine-based color production likely differs from that of other fishes, as well as the nudibranch example with which they are most similar; we examine possible mechanisms more deeply in the next section.

In addition to our dehydration-rehydration experiments above, the response of our specimens to chemical fixation supports our assertion that pale cells are involved in producing a structural blue in the ribbontail stingray. Blue spots from adult specimens fixed and stored for ≈4 years in a buffer solution lost their blue color with time (Figure S4a,b, Supporting Information). Such color loss is common in fixed specimens with structural color, attributed to architectural or refractive index changes that occur as a result of fixation.[56–59] In our long-fixed ribbontail stingray samples, ultrastructural characterization showed that pale cell nano-vesicles in blue regions were less densely arranged than in more

© 2024 The Authors. Advanced Optical Materials published by Wiley-VCH GmbH

freshly-fixed specimens, and intravesicular guanine crystals were rare (Figure S4c,d, Supporting Information). In contrast, tissue from samples frozen for the same amount of time remained blue (albeit comparatively dark), with SEM of isolated skin verifying the presence of guanine crystals. Furthermore, the freshly-fixed spots from the juvenile specimen remained electric blue for several weeks after fixation with glutaraldehyde and therefore we suppose their ultrastructures (Figure S4c, Supporting Information) are close to natural tissue architectures. The exact cause of color loss in long-fixed tissue remains to be identified, but these observations argue that the spacing of nano-vesicles and/or the presence of guanine nano-crystals (or the composite of crystals and vesicles, see below) are vital for color production in ribbontail stingray, a hypothesis we test below.

2.3. Coherent Scattering from Core–Shell Photonic Glass Ultrastructure of Blue Spots

In natural structural colors, the color produced (i.e., wavelengths scattered by the nanostructures) and the color saturation (i.e., the intensity of color) depend on the morphology and arrangement of the scatterers and their refractive index relative to their surrounding medium.[60,61] When nanostructures have a long-range order, as in a photonic crystal, the light waves interfere coherently to produce angle-dependent color (iridescence). Iridescent colors from ordered nanostructures are widespread in nature—on the feathers of hummingbirds (multilayer stacks of melanin in a keratin matrix); elytra of diamond weevils (a photonic crystal arrangement of voids in chitin); skin of bony fishes (multilayer stacks of guanine platelets in iridophore cells) [62]; petals of flowers (diffraction gratings on petal surfaces) [63] and others. In contrast, when nanostructural arrangements are completely random, incident light waves scatter incoherently (e.g., Rayleigh or Tyndall scattering) and the reflected color is non-iridescent. Accordingly, it was long believed that non-iridescent natural colors are caused only by incoherent scattering from zero-order architectures (e.g., colloidal nano-spheres in damselfly integuments,[64] air-filled structures of alveoli in giant blue swallowtails,[65] the spongy keratin–air matrix of feather barbs [48,66]). This hypothesis was recently disproved by Prum et al.,[67–69] who performed 2D Fast Fourier Transform analyses on transmission electron micrographs of structural colored tissues to calculate dominant frequency components in the arrangement of nanostructural arrays, revealing aspects of order and disorder otherwise imperceptible in direct observations of electron microscope images. Since electron density (gray-scale) variation in properly-stained electron micrographs is indicative of differences in refractive index (RI), the patterns observed in resultant 2D FFT power spectra can be used to distinguish between completely ordered, quasi-ordered, and disordered structures, with peak widths corresponding to the spatial frequency of refractive index differences. In this way, Prum et al.[57,59,67] were able to confirm that the keratin–air structures in feather barbs and nanospheres in damselfly integuments exhibit a quasi- or short-range order in spatial scales comparable to visible wavelengths to produce a coherently-scattered, but viewing angle-independent color.

We apply a similar approach to Prum et al.[57] in our examination of ribbontail stingray micrographs, using 2D FFT analysis to explore the degree of order and predicted optical appearance of tissues we observed in our anatomical characterizations. Nanovesicle arrays in pale cells showed a ring-like power spectrum (**Figure** 4a), confirming they are mono-disperse, quasi-ordered, and with a spatial periodicity that the Fourier power spectra predict produces a mean reflectance peak at a wavelength of 468 nm, closely corresponding to an electric blue color (Figure 4b). This supports our hypothesis that the spatial correlation between vesicles leads to constructive interference of blue light reflected from the nanostructural arrays in pale cells. Furthermore, the consistent FFT pattern observed from various TEM images—involving a nearly circular single Fourier ring—indicates that the spatial arrangement of vesicles in pale cells is isotropic, resembling a "direct" photonic glass ultrastructure.[70–72] This explains the origin of the distinct and angle-independent color of blue spots in the ribbontail stingray. A direct photonic glass consists of monodisperse colloidal structures in an isotropic disordered arrangement but with a short-range order and higher refractive index compared to the surrounding matrix. It is this material constellation that produces the interesting combination of color characteristics in ribbontail stingrays, where the structural correlations from the quasi-order of guanine-containing pale cell vesicles lead to coherent scattering of light, but the isotropic nature of the nanostructures results in angle-independence of the structural color.[73] As a counterpoint, in a poorly-preserved adult specimen where tissues had lost their blue hue, guanine crystals were lacking, vesicles were less densely packed (Figure S4d, Supporting Information), and the Fourier spectra from pale cell micrographs were filled disks rather than rings (indicating no structural order; Figure S5, Supporting Information), further illustrating that the quasi-order of guanine-containing vesicles is essential for the blue color production.

Recently, it was suggested that guanine crystals in the scales of Koi fish *Cyprinus rubrofuscus* and the skin of white widow spiders *Latrodectus pallidus* crystallize from an amorphous precursor distributed within vesicles.[50,51] If guanine crystal maturation also takes place in the same way in ribbontail stingray pale cells, we suppose that the refractive index of intravesicular space and guanine depends upon the stage of crystal development. The presence of guanine crystals inside vesicles thus results in a non-monotonous variation in refractive index, with most intravesicular space (i.e., the region between guanine and outer vesicular membrane) having an intermediate refractive index when compared to the guanine "cores" of vesicles and the surrounding cytoplasm, and where the guanine cores may act as the dominant scattering sites. As such, in matured vesicles, the guanine nanocrystals' morphology, high refractive index, and lack of defined orientation may help to significantly enhance scattering in all directions, while the quasi-order of the vesicles provides the resonance that is necessary for angle-independent blue structural color (Figure 4c). Also, the fact that vesicles do not appear to coalesce suggests that an unknown mechanism maintains the stability of the colloidal system, perhaps the structure and material properties of the cytoplasm and/or electrostatic repulsion between the vesicles. The mechanism determining crystal shape/growth is still unclear, but our observations of a consistent vesicle morphology in juvenile and adult individuals indicate that the stability of the vesicular core–shell ultrastructure is preserved throughout ontogeny. Thus, it

© 2024 The Authors. Advanced Optical Materials published by Wiley-VCH GmbH

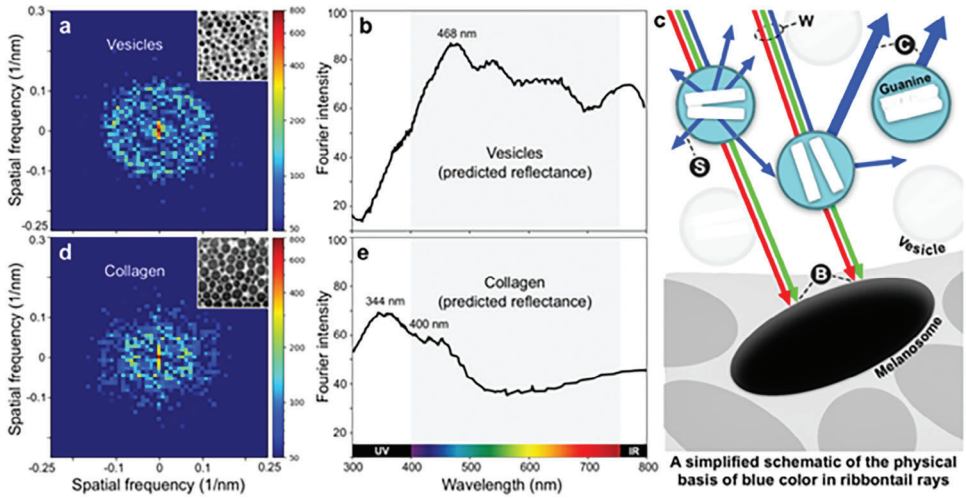

Figure 4. Coherent scattering of short wavelengths from the blue spots: a) 2D-FFT analysis of TEM images of vesicles shows a single ring-like spectrum demonstrating that the vesicles are arranged in a quasi-order. b) The predicted reflectance spectrum shows peaks in the blue wavelength region closely corresponding to wavelengths reflected by the real skin (see Figure 2). c) The schematic shows the possible physical mechanisms of blue color production by ribbontail stingray skin: as incident white light [W] passes through the pale cells, the high refractive index guanine nanoplatelets in vesicles scatter [S] short wavelengths strongly in all directions, while long wavelengths are weakly scattered. Furthermore, (a,b) the quasi-order of the vesicles leads to a strong coherent scattering [C] of blue wavelengths, aided by broadband absorption [B] of longer and multiply-scattered wavelengths by melanosomes. d) The lower collagen layer also showed a single ring-like 2D-FFT spectrum, however, e) the predicted peaks occurred in the UV region.

appears that the vesicles act as stable containers for the scattering guanine cores, while the dense cytoplasm controls the inter-vesicular spacing, critical for controlling the wavelengths scattered.[73-75]

It is conceivable that the thick collagen fiber bundles in the lower dermis of the skin also contribute to the blue color of ribbontail stingray. In some bird and mammalian skins, a thick layer of quasi-ordered collagen fibers scatters light coherently to produce structural blue colors.[58,76] Similarly, in electric rays (*Torpedo ocellata*, a batoid relative of ribbontail stingray), it was suggested that collagen fibers are responsible for the bright blue spots on the skin.[2] In the ribbontail stingray, 2D FFT spectra showed that the arrangement of collagen fibers in the lower dermis is also quasi-ordered, however, the mean predicted reflectance from the Fourier power spectra showed peaks in the UV region (≈344 nm), and in the violet region (≈400 nm) of the visible spectrum (Figure 4d,e). Moreover, the architecture of lower dermis collagen fiber bundles is almost identical in both blue and non-blue regions of the skin, only slightly thicker in the non-blue region, indicating that the blue color cannot originate from the collagen layers. In addition, the pervasiveness of melanosomes—in a dense layer of black melanophores at the bottom of the upper dermis in blue skin regions, and brown melanosomes in the upper dermis in the non-blue regions should restrict most incident wavelengths (including blues) from even reaching the collagen bundles in the lower dermis, with the melanosomes also probably absorbing any light that would be back-scattered from the collagen bundles (Figure 4c). Rather, our FFT predictions and skin reflectance measurements, argue that the extensive lower dermis collagen layer is responsible for the distinct UV reflectance from all skin regions (Figure 1d, 2), and which proved extremely robust to different specimen storage and processing conditions (e.g., present even in spots that had been dried or had their top layer removed).

Although photonic glass ultrastructures (e.g., the quasi-order of pale cell vesicles) result in strong scattering, their comparative disorder also translates to poor spectral selectivity or less-saturated structural color.[77] In ribbontail stingrays, this was evidenced by the pale blue of spots when viewed on a white background. Our tissue isolation experiments and characterizations indicate that spectral selectivity is improved by adding a black material in close association, namely the ubiquitous black melanophores within the pale cell layer in the upper dermis of blue tissue regions. While the melanophores with their horizontal processes deeper in the tissue absorb wavelengths transmitted through the pale cells and scattered from the lower collagen layer, the intracellular melanosomes distributed throughout the pale cell layer should absorb incoherently- or multiply-scattered long wavelengths, enhancing the saturation of the blue color [34,77,78] (Figure 4c). We expect that the high aspect ratio of ellipsoidal melanosomes in black melanophores also helps to further enhance broadband absorption.[79] Therefore, we argue that a combination of structural scattering from vesicles with randomly oriented guanine cores and broadband absorption from melanin pigments is crucial for the strong non-iridescent electric blue color of ribbontail stingray skin. This unique nano-structural skin architecture represents an interestingly disordered arrangement for color production, with the mechanism not only demanding the evolution of the unusual pale cell type but also its intimate association with melanophores. Our demonstration that certain tissue components and structural arrangements are necessary to produce the ribbontail stingray's blue color also argues that subtle structural modifications to the observed tissue nanoarchitectures may be the root of the natural color variation we observed in the field (Figure 1a). The presence of pale cells, even in non-blue areas, suggests that they may have (or have had) some other tissue function, but it was their evolutionary co-optation into a structural partnership with melanophores that gave rise to

© 2024 The Authors. Advanced Optical Materials published by Wiley-VCH GmbH

the novel and ecologically important tissue color. Understanding pale cell origins and their prevalence in other species and tissues will therefore be key for understanding the evolution of structural color in elasmobranch skin, but also for designing biomimetic structural blues.

3. Conclusion

This first report on the basis of skin color in elasmobranchs also demonstrates a new mechanism of guanine-based structural color production in animals. Although guanine-based methods for generating blue hues are quite common among natural structural color systems, the light-matter interactions involved are surprisingly diverse. For example, whereas the blue coloration of the mantle tissue of nudibranch molluscs is the result of incoherent Rayleigh scattering from disordered vesicular nanocrystals,[80] the blues of bony fish skin are due to multilayer interference from stacks of large guanine platelets.[54] In contrast, we show that the blue spots of ribbontail stingrays are the result of coherent scattering from a quasi-ordered arrangement of nano-vesicles with guanine nanoplatelets in pale cells, coupled with broadband absorption by melanophores. In relation to other guanine-based natural blues, the robust and angle-independent structural blue color of ribbontail stingray underlines that crystal morphology, ordering, and tissue associations offer a multivariate palette for producing color through evolution. Given that biogenic guanine crystals can also vary in their purity (often involving surprisingly large amounts of other purines [81]) and that the mechanisms underlying elasmobranch skin coloration remain largely unexplored, research into the composition of guanine crystals in ribbontail stingrays and other elasmobranchs, and into the development, function(s) and prevalence of pale cells will bring new perspectives on the early evolution and diversity of color production mechanisms in vertebrates.

Pale cells, the source of blue color in ribbontail stingrays, boast a unique morphology relative to other structural color-producing cells in fishes, but their use of guanine as a scattering material argues they may, in fact, be modified iridophores. Our results demonstrate that the nanoscale of guanine platelets and the spacing of their vesicles are key for strong angle-independent blue color production. Since the blues produced by bony fish iridophores are due to multilayer interference from large, agglomerated guanine crystals, pale cells could represent iridophores where the developmental process has been somehow truncated to produce smaller crystallites, perhaps through heterochrony or restrictions on crystal growth and vesicle coalescence.[51,52] The ontogeny of pale cells, but also the composition of their vesicular- and intervesicular-matrices, are therefore important targets for future work, as they could offer clues to the matrix-based control of crystal growth and the evolutionary roots of structural color in elasmobranchs (e.g., whether components of the more-common non-blue tissues were co-opted to produce blues), but also core factors in the evolution of iridophores and vertebrate structural color. The indication that strong blue and UV reflections occur in different skin tissue layers in ribbontail stingrays and may serve distinct ecological functions (conspecific and anti-predator signaling vs UV-camouflage) also argues that different selective pressures may have driven the evolution of local skin anatomy in elasmobranch fishes.

The electric blue skin of ribbontail stingray serves as a unique biomimetic model for color-saturated core–shell photonic glasses, showcasing that bright and robust coloration is possible, even from less controlled architectures. Artificial colloidal systems such as photonic glasses, despite having inherent poor saturation, can be excellent optical materials with high degrees of control, because they allow precise manipulations of nanostructure and color. Therefore, there is considerable interest in fabricating colloidal material architectures to produce bright angle-independent structural colors.[70–75,77,82] In the presence of a broadband absorber, by modulating the size of cores and shells, their spatial arrangement, and refractive indices, the structural colors of the biomimetic optical system can be tuned.[74] Additionally, the anisotropic shape of highly reflective crystal cores offers unique avenues for further color tuning. For instance, employing magnetically or electrically charged anisotropic scatterers as cores allows precise local control of core orientation by external fields, resulting in a variety of color patterns.[83] Such modulation of nanostructure orientations as well as their spatial order (or disorder) also facilitates a shift between non-iridescence and iridescence, thus inspiring a variety of applications in adaptive and sustainable textiles, flexible displays, screens, and sensors.

4. Experimental Section

Sample Collection and Handling: Several fresh specimens of the blue-spotted ribbontail stingray *T. lymma*, originating opportunistically from commercial fisheries between May 2017 and June 2022, were used in this study. Specimen data were collected following the protocol by Mollen.[84] Specimens examined included: one adult male (TALY1; ≈23 cm DW, 28 cm DL, 60.4 cm TL), western Indian Ocean, Kenya; one adult male (TALY2; ≈21 cm DW, 25 cm DL, 59 cm TL) and one adult female (TALY3; ≈26.0 cm DW, 72.5 cm TL), from northeast Singapore waters between Pulau Ubin and Changi; and one juvenile female (TALY4, *ex* ERB 1300; ≈14.9 cm DW, 35.7 cm TL) from Indonesia, Jakarta. The majority of data reported in the study come from the latter two specimens (TALY3-4); as TALY1-2 had been frozen for several years by the time of observation, these largely provided a preliminary understanding of the tissue. DW: disc width; DW: disc length and TL: total length.

As a result, for nearly all experiments and microscopy, tissue samples were collected and processed as soon as possible after the natural death of animals (e.g., occurring during normal fishing operations, live transport, or zoo husbandry). No animals were euthanized for this study. The live animal optical studies (see below) were performed on TALY4, an aquarium specimen in normal husbandry conditions. The water level of the animal's container was lowered so that its upper dorsum was only barely covered with water for a very short period of time, without preventing the animal from breathing normally. Spectroscopic measurements were rapidly acquired and then the water level was immediately restored (see below). This procedure was in compliance with EU directive 2010/63/EU on the protection of animals used for scientific purposes and also avoided the need to physically handle the animal. Permission to handle animal byproducts was obtained by the Max Planck Institute of Colloids and Interfaces for research purposes (permit no: DE 12 054 0006 21) and ethics approval (reference number: A-0741) was obtained from the Animal Research Ethics Sub-Committee at the City University of Hong Kong. Sometime later, TALY4 died during normal zoo husbandry procedures, offering the opportunity to make measurements on the same animal pre- and post-mortem.

Macroscale Observations and Light Microscopy: Macroscopic visual observations and digital photography (Canon 600D DSLR handheld camera) were carried out in sunlight (TALY3) and lab (TALY3-4) conditions to examine color differences between blue and non-blue regions of the skin.

© 2024 The Authors. Advanced Optical Materials published by Wiley-VCH GmbH

Color Measurements: Optical studies were performed on a live juvenile (TALY4) and dead adult ribbontail stingrays (TALY3-4) using a customized setup including a light source (DH-2000-BAL, Ocean Insight), a spectrometer (OCEAN-HDX-XR, Ocean Insight), and Y-type compound optical fiber for transmission of the light source and collection of the reflected spectra from the skin surface. All measurements were conducted with the tissue immersed in water, with the surface of the tissue 6–10 mm below the water surface. The optical probe was dipped at least 3 mm below the water surface and reflectance measurements were carried out at maximum signal intensity. At the maximum intensity, the working distance was ≈3 mm, with the probe spot size was ≈3 mm in diameter. For pre-measurement calibration of our light source, we simulated sunlight/daylight by selecting a preset (D65) provided by the manufacturer's software program, OceanView, and used the "Diffuse Reflectance Standard (WS-1)" provided by Ocean Insight for white color calibrations. The collected spectra were extracted using OCEANVIEW (Ocean Insight) and then plotted using the matplotlib module in Python.

De/Rehydration Studies: To study the effect of hydration on blue skin color, the darkened blue spots of frozen adult specimens (TALY3) were cut and immersed in DI water. Once the spots had returned to a brighter blue hue following rehydration, the outer skin layers (≈0.4 mm) were gently peeled off in water, affixed upside down onto a black carbon tape, and subjected to multiple de/rehydration cycles by dehydrating the tissue in the electron microscope while simultaneously imaging, followed by rehydration of the tissue in the laboratory; this cycle was repeated each day for 4 days and then again after 6 months. Images of all color changes were recorded using a handheld digital camera. Images of fresh and dehydrated tissue were also performed with an AxioZoom.v16 stereomicroscope equipped with a white LED light and a custom-made on-stage incubator where humidity could be monitored and decreased using an airflow between an inlet and outlet.

Environmental Scanning Electron Microscopy (ESEM) and Energy Dispersive X-Ray Analysis (EDX): ESEM and EDX were performed to provide information on tissue ultrastructure and composition. Outer skin layers (≈0.4 mm) of frozen ribbontail stingray were isolated in water and gently affixed upside down onto black carbon tape. The morphology of the inverted tissue (with melanosome granules and guanine platelets detectable on the surface) was then observed at high resolution using an environmental scanning electron microscope (ESEM, Quattro S, Thermo Fisher Scientific, FEI Deutschland GmbH, Germany) with a secondary electron (SE) detector operated at 5 kV with a 5.9 mm working distance and low vacuum (0.75 torr pressure). The elemental composition of the samples was obtained using an EDX detector at 30000× magnification at 15 kV.

Micro-Computed Tomography: To investigate the presence of radio–opaque structures contributing to tissue color production, micro-computed tomography of fixed samples was performed at the Max–Planck Institute of Colloids and Interfaces in Potsdam–Golm (MPIKG, Germany) with an RX Solutions EASYTOM µCT scanner (RX Solutions, Chavanod, France). Scans were performed with helix scan sample rotation, at a tube voltage of 80–100 kV, a tube current of 117 µA, 15 W, and an isometric voxel size of <10 µm, with a beam hardening correction algorithm applied during image reconstruction. Scans showed no radio–opaque structures in the skin (data not included in the discussion).

Raman Spectroscopy: To provide further local composition information, confocal Raman spectroscopy was performed (alpha300R, WITec, Ulm) on isolated blue tissue from a frozen specimen, inverted onto carbon tape (i.e., with the tissue's deep surface facing outward), using a 532 nm laser source and a ×20 objective lens (Zeiss EC Epiplan-Neofluar Dic 20x / 0.5). An integration time of 1 s, accumulations 70–200 times, laser power of 12 mW, and a grating of 600 g mm^{-1} were used for acquisition. The spectrometer was calibrated using a silicon wafer sample. WITec Project Five 5.2 and OriginPro 2020 were used for filtering, analyzing, and plotting the data.

Transmission Electron Microscopy (TEM): Soon after the death of the fish, skin samples of ≈5 mm^3 including both the blue spot and adjacent non-blue area, were collected and fixed in Karnovsky's solution (2% PFA, 2.5% GA, buffered in 0.1 M PBS) for 2 h on a shaker at room temperature, and subsequently stored at 4 °C. The samples were shipped to the Medical University of Innsbruck, where they were further processed for TEM, to provide nanoscale observations of tissue morphology; the remaining voucher material was deep frozen at the Max Planck Institute of Colloids and Interfaces (MPICI, Potsdam, Germany). The shipped samples were cut into smaller pieces, each containing the blue spot and adjacent non-blue tissue. Samples were rinsed in sodium cacodylate buffer and post-fixed in 0.5% osmium tetroxide and 1% potassium ferricyanide in distilled water overnight at 4 °C. They were rinsed again, dehydrated in graded ethanol series, and embedded in EPON resin (#45359, Sigma–Aldrich, Austria). Vertical ultrathin sections (90 nm) were cut with an ultradiamond knife (Diatome, Biel, Switzerland), mounted on dioxane formvar-coated slot grids (#PYSL2010S-CU, Science Services, München, Germany), and stained with 1% uranyl acetate and lead citrate.[85] Ultrathin sections were examined with a Philips CM 120 transmission electron microscope at 80 kV (FEI, Eindhoven, The Netherlands), equipped with a MORADA digital camera. Size measurements of observed nanostructures were carried out using the microscope's iTEM software (Olympus SIS, Münster, Germany).

FFT Analysis: Square sections were extracted from multiple individual TEM images of vesicles and contrast-adjusted using ImageJ software to enhance the distinction between tissue components (i.e., vesicles relative to extra-vesicular background). To look for order and pattern in the tissue organization, 2D FFT analysis was performed using the scipy module in Python to obtain the FFT spectra of the vesicles. Similarly, the FFT spectra of collagen fibers from TEM images of the lower dermis were obtained. Using refractive index (RI) values of 1.8[86] and 1.42[87] for melanosomes and collagen respectively, and the pixel intensity contrast of different tissue elements from TEM images, the RI values of vesicles and pale cell cytoplasm were estimated to be 1.35 and 1.3. Using these values histograms were generated from the grayscale 2D FFT spectra to obtain the weighted mean refractive index of pale cells and collagen bundles. Radial mean data of Fourier intensity and wavelength (= 2 × RI/spatial frequency) were obtained from the grayscale 2D FFT spectra, the data were normalized from 0–100 in the visible wavelength range, and the predicted reflectance spectra were plotted using the matplotlib module in Python, providing estimates for the colors produced by specific tissues as a function of their nanostructure.

Ethics Approval Statement: Permission to handle animal byproducts was obtained by the Max Planck Institute of Colloids and Interfaces for research purposes (permit no: DE 12 054 0006 21) and ethics approval (reference number: A-0741) has been obtained from the Animal Research Ethics Sub-Committee at the City University of Hong Kong.

Supporting Information

Supporting Information is available from the Wiley Online Library or from the author.

Acknowledgements

The authors acknowledge Arie de Jong and Jeffrey de Pauw from the Netherlands and Shu Hui Hiew from Nanyang Technological University, Singapore for their support in securing fresh material of ribbontail stingray. The authors acknowledge Susann Weichold and Cécile Bidan, Max Planck Institute of Colloids and Interfaces, Germany for their support with ESEM and optical measurements. The authors thank A. Knab and Ch. Seifarth for technical assistance. The authors thank Joana Carvalho for the ribbontail stingray and skin illustration in Figure 3. The authors also thank Dvir Gur, Mathias Kolle, and Benjamin Palmer for useful discussions during the early development of this work, as well as Peter Fratzl for his support and insights throughout. The work was funded in part by an HFSP Program Grant (RGP0010-2020) and a General Research Fund GRF Grant from the Research Grants Council of the Hong Kong Special Administrative Region, China (CityU11102022) to MND.

Open access funding enabled and organized by Projekt DEAL.

© 2024 The Authors. Advanced Optical Materials published by Wiley-VCH GmbH

Conflict of Interest

The authors declare no conflict of interest.

Author Contributions

V.A.S and M.B. contributed equally to the study. M.D., S.A., and V.A.S. conceived and designed the study. F.M. provided the specimens. A.M. conducted the field studies. V.A.S. and K.T. conducted the optical and scanning electron microscopy studies. M.B., S.R., and H.R.H. conducted the histology, epi-illumination microscopy, and transmission electron microscopy studies. V.A.S. and S.A. conducted the color, EDX, and Raman spectroscopy studies. V.A.S conducted the 2D FFT analysis. V.A.S., M.B., S.A., and M.D. contributed to the interpretation of results. The manuscript was written by V.A.S, M.B., A.M., and M.D. with inputs from all the authors.

Data Availability Statement

All data and code that support the findings of this study are available in a publicly available online repository FigShare at https://doi.org/10.6084/m9.figshare.25206671.

Keywords

chromatophore, elasmobranch, guanine, non-iridescence, quasi-ordered nanostructure, scattering

Received: August 7, 2023
Revised: January 10, 2024
Published online: March 1, 2024

[1] T. Caro, *Bioscience*. **2005**, *55*, 125.
[2] J. T. Bagnara, P. J. Fernandez, R. Fujii, *Pigm. Cell Res.* **2007**, *20*, 14.
[3] K. D. L. Umbers, *J. Zool.* **2013**, *289*, 229.
[4] W. H. Longley, *J. Exp. Zool.* **1917**, *23*, 533.
[5] K. Lorenz, *Proc. R. Inst. Gr. Brit.* **1962**, *39*, 382.
[6] N. J. Marshall, *Philos. Trans. R. Soc. Lond. B Biol. Sci.* **2000**, *355*, 1243.
[7] R. Fujii, in *International Review of Cytology*, (Eds. K. W. Jeon, M. Friedlander, J. Jarvik), Academic Press, Cambridge **1993**. p. 191.
[8] R. Fujii, *Pigm. Cell Res.* **2000**, *13*, 300.
[9] J. T. Bagnara, J. Matsumoto, *The Pigmentary System: Physiology and Pathophysiology*, Wiley-VCH, Weinheim, Germany **2006**, 11, https://doi.org/10.1002/9780470987100.
[10] P. Salis, T. Lorin, V. Laudet, B. Frédérich, *Trends Genet.* **2019**, *35*, 265.
[11] D. A. Ebert, H.-C. Ho, W. T. White, M. R. De Carvalho, *Zootaxa*. **2013**, *3752*, 5.
[12] P. Last, G. Naylor, B. Séret, W. White, M. Stehmann, M. de Carvalho, *Rays of the World*, Csiro Publishing, Clayton, Australia **2016**.
[13] C. Niebuhr, *Descriptiones animalium avium, amphibiorum, piscium, insectorum, vermium; quae in itinere orientali observavit Petrus Forskål. Prof. Haun. post mortem auctoris editit Carsten Niebuhr. Adjuncta est material medica Kahirina atque tabula maris rubri geographica*, Mölleri, Hauniae, 1775, https://doi.org/10.5962/bhl.title.63873.
[14] P. R. Last, W. T. White, G. Naylor, *Zootaxa*. **2016**, *4147*, 377.
[15] O. R. O'Shea, M. Thums, M. Meekan, M. van Keulen, presented at *Physical and Biological Effects Associated with Stingray Foraging Behaviour at Ningaloo Reef, Western Australia*, Vancouver, Canada, Aug, **2012**.
[16] T. F. Dabruzzi, W. A. Bennett, J. L. Rummer, N. A. Fangue, *Hydrobiologia*. **2013**, *701*, 37.
[17] A. J. McIvor, J. L. Y. Spaet, C. T. Williams, M. L. Berumen, *ICES J. Mar. Sci.* **2022**, *79*, 1604.
[18] A. Chin, P. M. Kyne, T. I. Walker, R. B. McAULEY, *Glob Chang Biol.* **2010**, *16*, 1936.
[19] C. P. Brinton, M. C. Curran, *Mar. Freshw. Res.* **2017**, *68*, 1716.
[20] A. P. B. Martins, M. R. Heupel, S. L. Bierwagen, A. Chin, C. Simpfendorfer, *PLoS One*. **2020**, *15*, e0228280.
[21] C. Elston, P. D. Cowley, T. S. Murray, M. C. Parkinson, *Biodivers. Conserv.* **2023**, *32*, 181.
[22] E. J. Hochberg, S. A. Peltier, S. Maritorena, *Coral Reefs*. **2020**, *39*, 1377.
[23] B. J. Russell, H. M. Dierssen, E. J. Hochberg, *Remote Sens.* **2019**, *11*, 1757.
[24] J. T. O. Kirk, *Hydrobiologia*. **1985**, *125*, 195.
[25] S. Kinoshita, S. Yoshioka, J. Miyazaki, *Rep. Prog. Phys.* **2008**, *71*, 076401.
[26] N. S. Hart, T. D. Lamb, H. R. Patel, A. Chuah, R. C. Natoli, N. J. Hudson, S. C. Cutmore, W. I. L. Davies, S. P. Collin, D. M. Hunt, *Mol. Biol. Evol.* **2020**, *37*, 811.
[27] E. Garza-Gisholt, R. M. Kempster, N. S. Hart, S. P. Collin, *Brain Behav Evol.* **2015**, *85*, 217.
[28] S. M. Theiss, T. J. Lisney, S. P. Collin, N. S. Hart, *J. Comp. Physiol. A Neuroethol. Sens. Neural Behav. Physiol.* **2007**, *193*, 67.
[29] N. J. Marshall, F. Cortesi, F. de Busserolles, U. E. Siebeck, K. L. Cheney, *J. Fish Biol.* **2019**, *95*, 5.
[30] J. Marshall, *Curr. Biol.* **2017**, *27*, R494.
[31] U. E. Siebeck, N. J. Marshall, *Vision Res.* **2001**, *41*, 133.
[32] G. S. Losey, T. W. Cronin, T. H. Goldsmith, D. Hyde, N. J. Marshall, W. N. McFarland, *J. Fish Biol.* **1999**, *54*, 921.
[33] R. Chadyšiene, A. Girgždys, *J. Environ. Eng. Landsc. Manag.* **2008**, *16*, 83.
[34] I. C. Cuthill, J. C. Partridge, A. T. D. Bennett, S. C. Church, N. S. Hart, S. Hunt, in *Advances in the Study of Behavior*, (Eds. P. J. B. Slater,J. S. Rosenblatt, C. T. Snowdon, T. J. Roper), Academic Press, Cambridge **2000**. pp. 159–214.
[35] M. D. Shawkey, G. E. Hill, *J Exp Biol.* **2006**, *209*, 1245.
[36] J. D. Forster, H. Noh, S. F. Liew, V. Saranathan, C. F. Schreck, L. Yang, J.-G. Park, R. O. Prum, S. G. J. Mochrie, C. S. O'Hern, H. Cao, E. R. Dufresne, *Adv. Mater.* **2010**, *22*, 2939.
[37] M. D. Shawkey, L. D'Alba, J. Wozny, C. Eliason, J. A. H. Koop, L. Jia, *Zoology.* **2011**, *114*, 59.
[38] D. Ge, L. Yang, G. Wu, S. Yang, *J. Mater. Chem.* **2014**, *2*, 4395.
[39] M. M. Giusti, R. E. Wrolstad, *Curr. Protoc. Food Anal. Chem.* **2001**, *00*, F1.2.1.
[40] H. G. Frohnhöfer, J. Krauss, H.-M. Maischein, C. Nüsslein-Volhard, *Development.* **2013**, *140*, 2997.
[41] L. D. Faílde, R. Bermúdez, F. Vigliano, G. A. Coscelli, M. I. Quiroga, *Tissue Cell.* **2014**, *46*, 334.
[42] J. Oeffner, G. V. Lauder, *J. Exp. Biol.* **2012**, *215*, 785.
[43] M. V. Ankhelyi, D. K. Wainwright, G. V. Lauder, *J. Morphol.* **2018**, *279*, 1132.
[44] M. E. Rawles, *Physiol. Rev.* **1948**, *28*, 383.
[45] J. D. Taylor, B. J. T. D. Chromatophoies, *Am. Zool.* **1972**, *12*, 43.
[46] Š. Moudříková, L. Nedbal, A. Solovchenko, P. Mojzeš, *Algal Res.* **2017**, *23*, 216.
[47] A. Jantschke, I. Pinkas, A. Hirsch, N. Elad, A. Schertel, L. Addadi, S. Weiner, *J. Struct. Biol.* **2019**, *207*, 12.
[48] D. L. Fox, *Animal Biochromes and Structural Colours*, University of California Press, Berkeley. CA, **1976**.
[49] Y. Kamishima, *Proc. Jpn. Acad. Ser. B Phys. Biol. Sci.* **1978**, *54*, 634.
[50] D. Gur, Y. Politi, B. Sivan, P. Fratzl, S. Weiner, L. Addadi, *Angew. Chem. Int. Ed. Engl.* **2013**, *52*, 388.
[51] A. Wagner, V. Ezersky, R. Maria, A. Upcher, T. Lemcoff, E. D. Aflalo, Y. Lubin, B. A. Palmer, *Adv. Mater.* **2022**, *34*, 2202242.
[52] Z. Eyal, R. Deis, N. Varsano, N. Dezorella, K. Rechav, L. Houben, D. Gur, *J. Am. Chem. Soc.* **2022**, *144*, 22440.

© 2024 The Authors. Advanced Optical Materials published by Wiley-VCH GmbH

[53] E. J. Denton, *Philos. Trans. R. Soc. Lond. B Biol. Sci.* **1970**, *258*, 285.
[54] A. Levy-Lior, E. Shimoni, O. Schwartz, E. Gavish-Regev, D. Oron, G. Oxford, S. Weiner, L. Addadi, *Adv. Funct. Mater.* **2010**, *20*, 320.
[55] S. J. Dearden, A. Ghoshal, D. G. DeMartini, D. E. Morse, *Biol. Bull.* **2018**, *234*, 116.
[56] R. O. Prum, R. L. Morrison, *J. Morphol.* **1994**, *222*, 61.
[57] R. O. Prum, R. Torres, S. Williamson, J. Dyck, *Proc. R. Soc. Lond. B: Biolog. Sci.* **1999**, *266*, 13.
[58] R. O. Prum, R. Torres, *J. Exp. Biol.* **2003**, *206*, 2409.
[59] R. O. Prum, J. A. Cole, R. H. Torres, *J. Exp. Biol.* **2004**, *207*, 3999.
[60] L. Schertel, L. Siedentop, J.-M. Meijer, P. Keim, C. M. Aegerter, G. J. Aubry, G. Maret, *Adv. Opt. Mater.* **2019**, *7*, 1900442.
[61] G. Jacucci, S. Vignolini, L. Schertel, *Proc. Natl. Acad. Sci. U S A.* **2020**, *117*, 23345.
[62] S. Kinoshita, *Structural Colors in the Realm of Nature*, World Scientific, Singapore **2008**.
[63] H. M. Whitney, M. Kolle, P. Andrew, L. Chittka, U. Steiner, B. J. Glover, *Science.* **2009**, *323*, 130.
[64] C. W. Mason, *J. Phys. Chem.* **1926**, *30*, 383.
[65] J. Huxley, *Proc. R. Soc. Lond. B.* **1976**, *193*, 441.
[66] E. Finger, *Naturwissenschaften.* **1995**, *82*, 570.
[67] R. O. Prum, R. H. Torres, S. Williamson, J. Dyck, *Nature.* **1998**, *396*, 28.
[68] R. O. Prum, R. Torres, C. Kovach, S. Williamson, S. M. Goodman, *J. Exp. Biol.* **1999**, *202*, 3507.
[69] R. O. Prum, R. H. Torres, *Integr. Comp. Biol.* **2003**, *43*, 591.
[70] J. Ballato, J. Dimaio, A. James, E. Gulliver, *Appl. Phys. Lett.* **1999**, *75*, 1497.
[71] L. F. Rojas-Ochoa, J. M. Mendez-Alcaraz, J. J. Sáenz, P. Schurtenberger, F. Scheffold, *Phys. Rev. Lett.* **2004**, *93*, 073903.
[72] P. D. García, R. Sapienza, Á. Blanco, C. López, *Adv. Mater.* **2007**, *19*, 2597.
[73] S. Magkiriadou, J.-G. Park, Y.-S. Kim, V. N. Manoharan, *Phys. Rev. E Stat. Nonlin Soft Matter Phys.* **2014**, *90*, 062302.
[74] S. Magkiriadou, J.-G. Park, Y.-S. Kim, V. N. Manoharan, *Opt. Mater. Express.* **2012**, *2*, 1343.
[75] J.-G. Park, S.-H. Kim, S. Magkiriadou, T. M. Choi, Y.-S. Kim, V. N. Manoharan, *Angew. Chem. Int. Ed. Engl.* **2014**, *53*, 2899.
[76] R. O. Prum, R. H. Torres, *J. Exp. Biol.* **2004**, *207*, 2157.
[77] G. Shang, M. Eich, A. Petrov, *APL Photonics.* **2020**, *5*, 060901.
[78] Y. Takeoka, *J. Mater. Chem.* **2012**, *22*, 23299.
[79] A. L. Davis, K. N. Thomas, F. E. Goetz, B. H. Robison, S. Johnsen, K. J. Osborn, *Curr. Biol.* **2020**, *30*, 3470.
[80] S. Kawaguti, Y. Kamishima, *Biol. J. Okayama Univ.* **1964**, *10*, 83.
[81] N. Pinsk, A. Wagner, L. Cohen, C. J. H. Smalley, C. E. Hughes, G. Zhang, M. J. Pavan, N. Casati, A. Jantschke, G. Goobes, K. D. M. Harris, B. A. Palmer, *J. Am. Chem. Soc.* **2022**, *144*, 5180.
[82] K. Li, C. Li, H. Li, M. Li, Y. Song, *iScience.* **2021**, *24*, 102121.
[83] I. Mattich, J. Sendra, H. Galinski, G. Isapour, A. F. Demirörs, M. Lattuada, S. Schuerle, A. R. Studart, *Adv. Opt. Mater.* **2023**, *11*, 2300734.
[84] F. H. Mollen, *Zootaxa.* **2019**, *4571*, 295.
[85] E. S. Reynolds, *J. Cell Biol.* **1963**, *17*, 208.
[86] D. Stavenga, H. Leertouwer, D. Osorio, B. Wilts, *Light Sci. Appl.* **2015**, *4*, e243.
[87] D. W. Leonard, K. M. Meek, *Biophys. J.* **1997**, *72*, 1382.

© 2024 The Authors. Advanced Optical Materials published by Wiley-VCH GmbH